Physica D 476 (2025) 134633

Contents lists available at ScienceDirect

Physica D

journal homepage: www.elsevier.com/locate/physd

Supercontinuum generation in a few-mode liquid-core fiber

Lanh Chu Van [a], Hieu Le Van [b], Van Thuy Hoang [a],*

[a] Derpartment of Physics, Vinh University, 182 Le Duan, Vinh City, Nghe An, Viet Nam
[b] Faculty of Natural Sciences, Hong Duc University, 565 Quang Trung Street, Thanh Hoa City, Viet Nam

ARTICLE INFO

Communicated by Jesus Cuevas-Maraver

Keywords:
Supercontinuum generation
Nonlinear liquids
Noninstantaneous nonlinearity
Soliton
Multimode fiber
Polarization

ABSTRACT

Liquid-core fibers have been widely used for supercontinuum generation because of the high nonlinearity and high transparency of selected liquids. These fibers are fabricated using silica capillaries with micrometer core diameters infiltrated with nonlinear liquids. Since nonlinear liquids typically have a refractive index much higher than silica, this results in multimode guidance, especially in large core fibers. This study focuses on numerically investigating supercontinuum generation in a few-mode liquid-core (CS_2-core) fiber by using a commercial femtosecond laser with a central wavelength of 1560 nm and a pulse duration of 100 fs. The fiber has a core diameter of 5 μm and supports 24 polarized modes. Due to the high noninstantaneous nonlinearity of CS_2, the liquid-core fiber can achieve supercontinuum generation with higher coherence compared to solid-core fibers, for both linear and circular polarization. Additionally, this work investigates the interaction among the four polarized components of the first high-order mode (LP_{11}), pointing out the differences in power transfer between the polarized modes in the case of linear and circular polarization. The interaction between $HE_{11,x}$ and TM_{01} modes with all existing modes is also discussed.

1. Introduction

Supercontinuum (SC) generation is a spectral and temporal broadening of high-power laser pulses within nonlinear optical fibers and waveguides, driven by the interplay of nonlinearity and dispersion [1]. Recent advancements in fiber materials and fabrication technologies have enabled the production of SC with a broadened spectral bandwidth, spanning from ultraviolet (UV) to mid-infrared (mid-IR, from 3 μm to 20 μm). Consequently, fiber-based SC sources have become key factors in numerous applications, such as multi-photon imaging [2,3] and low-noise amplifier [4]. SC generation with extremely low shot-to-shot and temporal noises acts as broad bandwidth frequency combs, and thus, it is suitable to use for spectroscopy [5] and high-precision metrology [6]. In general, fiber materials include silica, silicon, hybrid glasses (e.g., telluride, chalcogenide), liquids and gases [7,8]. The main limitations of silica fibers are low nonlinearity and high absorption in UV and mid-IR range, thus silica fibers are only used for SC generation in visible and near-IR range with spectra limited around 2.5 μm [9,10]. In order to meet this limitation, silicon and chalcogenide fibers with high transmission in mid-IR range have been utilized for multi-octave spanning SC generation up to 5 μm [11] and 18 μm [12], covering the “fingerprint” absorption and vibration of various types of gas molecules for infrared spectroscopy applications. The drawback of chalcogenide fibers is difficulty in fabrication using the stack-and-draw method because of the glass crystallization and high sensitivity of viscosity to temperature changing [13]. Moreover, chalcogenide fibers do not have good mechanical resistance and get a quick optical aging process causing an increase in fiber absorption as well as changing their optical properties [14]. Another approach is to use hollow-core fibers filled with noble gases (e.g., argon and neon) that allow control of the fiber nonlinearity and dispersion by changing the gas pressure, thus, enabling control of the spectro-temporal properties of SC generation. The gas-core fibers have been used for broad SC with spectra ranging from UV up to 4 μm [15] as well as pulse compression up to attosecond duration [16]. Notwithstanding, the gas-core fibers typically require a laser pump with extremely high power (a few of μJ) because of the low nonlinearity of the selected gases and large core of the fibers [15].

Liquid-core fibers that are hollow core fibers infiltrated with liquids into the cores for light guidance are an attractive approach for SC generation [17,18] and other applications, such as optofluidic lasers, and sensors [19,20]. The advantage of liquid-core fibers involves an essential increase in the intensity of liquid-light interaction in the small fiber cores and the long optical path (along the fibers). Therefore, it enables the leveraging of unique properties of liquids, such as high nonlinearity, high transparency over a long bandwidth from visible to mid-IR, tuning the refractive index via changing temperature and pressure, to optimize spectro-temporal properties of SC generation [21]. Nonlinear

* Corresponding author.
E-mail address: thuyhv@vinhuni.edu.vn (V.T. Hoang).

https://doi.org/10.1016/j.physd.2025.134633
Received 13 July 2024; Received in revised form 31 January 2025; Accepted 12 March 2025
Available online 21 March 2025

Table 1
Supercontinuum generation in CS_2-core fibers.

Fiber	Core diameter (μm)	Pump wavelength (nm)	Peak power (kW)	Spectral bandwidth (nm)	Mode guidance	Refs
Step-index	2.3	1.55	12	1232–3189	Single-mode	[30]
PCF	1.8	1.55	3.9	1100–2500	Single-mode	[26]
Step-index	4.7	1.95	30	1100–2700	Single-mode	[17]
Step-index	3.9	1.56	13	1100–2100	3-modes (LP_{11} modes)	[31]
Tapered fiber	14→3	1.56	27	1000–3000	Single-mode	[23]
PCF	1.3	1.55	2	1280–2240	2-modes (LP_{01} modes)	[32]
Step-index	2.0	1.56	10	1000–3300	2-modes (LP_{01} modes)	[33]
Step-index	3.3	1.92	1	1280–2300	Single-mode	[21]
Step-index	5	1.56	15	1200–2400	Multimode (24 modes)	This work

liquids, such as carbon tetrachloride (CCl_4) and carbon disulfide (CS_2), have high transparency up to 6 μm [22], allowing to yield broad SC spectrum in mid-IR range [17,21,23]. Interestingly, unlikely glass, liquid nonlinearity is contributed by instantaneous Kerr (originated from the electron-bound response of liquid molecules) and, a major part, noninstantaneous nonlinearity (originated from reorientation of the liquid molecules via external electromagnetic field) [24], leading to hybrid soliton dynamics that allows for improvement of the coherence of soliton-based SC generation [17,25,26].

Nonlinear liquids typically have refractive index higher than silica [27], assuring light guidance by total internal refraction (TIR) and well-confining the light inside the fiber core to increase the nonlinear effects. However, the high refractive index, in turn, causes the few-mode and/or multi-mode guidance. Notwithstanding, most works have previously considered SC generation in liquid-core fibers with an assumption of single-mode operation and neglecting interaction between modes existing in liquid-core fibers. It is worth mentioning that few-mode and multi-mode fibers (MMFs) have gained interest in the scientific community due to their interesting properties over single-mode fibers. MMFs with large cores can yield high coupling efficiency with laser sources while enduring extremely high input energy without damage, thus making them ideal towards all-fiber, high power spectral density (PSD), and extremely broadband SC systems. Interaction between the existing modes not only changes the spectro-temporal properties of SC generation, but also provides an excellent tool with a high degree of freedom via a rich landscape of nonlinear dynamics to customize the nonlinear propagation for applications in, e.g., multiphoton microscopy and telecommunication [28,29].

Although liquid-core fibers have been widely utilized for coherent broadband SC generation, especially CS_2 filled fibers due to the high nonlinearity [17,21,25,26,30], most of the works consider only the single-mode guidance and neglect the effects of mode interaction (Table 1). The investigated fiber in this work is included.

Up to date, the exploration of nonlinear dynamics in few-mode liquid-core fibers remains relatively limited, and previous works considered the interaction of only specific modes, see Table 1. For instance, Scheibinger et al. engineered the fiber dispersion via initially exciting one of the 3 high-order modes (TM_{01}, TE_{01}, HE_{11}) to change the spectral property of SC generation in CS_2-core fibers [31]. Van et al. proposed highly birefringent liquid-core fibers and investigated coherence degradation resulting from interactions between polarization fundamental modes (LP_{01}) [33]. A theoretical model for synchronization of spatial modes in MMFs with high noninstantaneous nonlinearity (like CS_2) was proposed by Mei et al. [34].

Previous works have not investigated the interaction between all existing modes in liquid-core fibers, thus neglecting nonlinear phenomena that significantly contribute to spectro-temporal properties of SC generation, such as cross-phase modulation (XPM) and intermodal four-wave mixing (FWM). In addition, the interaction between the modes depends on their polarization state, resulting in coherence degradation of SC generation depending on the polarization of input laser pulses. These features have been studied for solid core fibers with Kerr nonlinearity [28]. Yet, mode interaction in liquid-core fibers with high noninstantaneous nonlinearity has not been thoroughly investigated. Therefore, investigation of SC generation in liquid-core fibers with multimode guidance is necessary to achieve a sufficient overview of light-matter interaction in the liquid media with high noninstantaneous nonlinearity.

In this work, we numerically study the interaction between the modes in the liquid-core fiber with high noninstantaneous nonlinearity for SC generation. Specifically, we thoroughly investigate the nonlinear dynamics, energy transfer, and coherence of SC generation within the interaction of the polarized components of the fundamental mode and the first higher-order modes. We also point out that noninstantaneous nonlinearity results in narrower spectral broadening while improving coherence. Additionally, we consider the energy transfer between all existing modes, focusing on the initially excited modes of $HE_{11,x}$ and TM_{01}.

2. Numerical modeling

Liquid-core photonic crystal fibers (PCFs) have been utilized to offer significant flexibility in optimizing dispersion for broadband SC generation [18,26,35]. However, these fibers necessitate a complex process to selectively infiltrate liquid into the core region [35,36]. Although modifying the cladding air-hole sizes in PCFs is an effective approach for tailoring fiber dispersion, this method is particularly suited for small cores, where the core size is comparable to the operating wavelengths. In contrast, for multimode fibers with large cores, dispersion is predominantly influenced by the material dispersion of the core rather than waveguide dispersion [18,35].

In this work, the liquid-core fiber is a step-index configuration that is realistically fabricated by using a micro-diameter silica capillary infiltrated with CS_2, as shown in Fig. 1(a). We work with CS_2 because of its high nonlinearity and high transparency [22]. This liquid has been widely used for SC generation (Table 1).

The core diameter is 5 μm. Silica has high attenuation in mid-IR (wavelengths longer 2.6 μm), while CS_2 is transparency up to 3 μm. The highest absorption at 2.2 μm is caused by the stretching and bending mode of the liquid molecules, Fig. 1(b).

Carbon disulfide has refractive indices higher than silica, resulting in effective light confinement within the core (i.e., low confinement loss) and multi-mode guidance at short wavelengths. The fiber has a V-parameter of 6.6 at 1560 nm, offering up to 24 vector modes (linearly polarized modes), corresponding to 7 scalar modes (LP_{mn}), as illustrated in Fig. 2. In particular, the fundamental mode (LP_{01}) includes 2 vector (linearly polarized) components of $HE_{11,x,y}$. The first high-order mode (LP_{02}) has 2 vector modes of $HE_{12,x,y}$. Other LP_{mn} modes consist of 4 components, such as LP_{11} comprises TM_{01}, TE_{01}, $HE_{21,\mathrm{even/odd}}$.

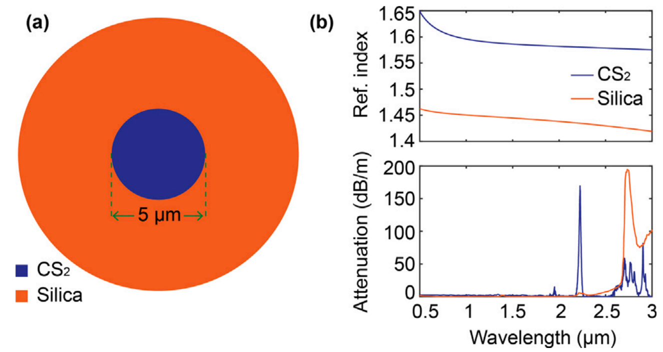

Fig. 1. (a) Fiber schemes with the core diameter of 5 μm. (b) Refractive index and attenuation of silica and CS_2 [17,22,37].

The vector modes of each LP_{mn} mode exhibit similar values of effective refractive index (RI); however, there is a significant difference in RI between the LP_{mn} modes, as shown in Fig. 3(a). For example, the difference in RI between LP_{01} and LP_{11} is 0.015, indicating that the fundamental mode is distinct from the high-order modes. Consequently, it is possible to selectively excite only the desired mode.

The liquid-core fiber has low birefringence, meaning that the polarized modes of each LP_{mn} have the same dispersion curve and loss, as shown in Fig. 3(b,c). The fundamental mode LP_{01} and high-order mode LP_{11} have one zero-dispersion wavelength (ZDW) at 1.85 μm and 1.55 μm, respectively. LP_{41} mode shows an all-normal dispersion, while other high-order modes have two ZDWs. Fiber loss consists of confinement loss and material loss from CS_2 and silica in the cladding. High-order modes have a high loss at longer wavelengths due to higher confinement loss. Notably, LP_{12} and LP_{31} do not exist at wavelengths longer than 2.1 μm because of extremely high confinement loss. Similarly, LP_{41} does not exist at wavelengths longer than 1.7 μm.

In the case of circular polarization, the fiber modes are calculated by combining the linearly polarized modes [38]. For instance, the fundamental and the first high-order modes with circular polarization are provided in Eq. (1):

$$\begin{aligned} \mathbf{F}_{11}^{+} &= \left(\mathbf{HE}_{11,x} + i\mathbf{HE}_{11,y}\right)/\sqrt{2} & \mathbf{F}_{11}^{-} &= \left(\mathbf{HE}_{11,x} - i\mathbf{HE}_{11,y}\right)/\sqrt{2} \\ \mathbf{F}_{21}^{+} &= \left(\mathbf{HE}_{21,\mathrm{even}} + i\mathbf{HE}_{21,\mathrm{odd}}\right)/\sqrt{2} & \mathbf{F}_{21}^{-} &= \left(\mathbf{HE}_{21,\mathrm{even}} - i\mathbf{HE}_{21,\mathrm{odd}}\right)/\sqrt{2} \\ \mathbf{F}_{T21}^{+} &= \left(\mathbf{TM}_{01} - i\mathbf{TE}_{01}\right)/\sqrt{2} & \mathbf{F}_{T21}^{-} &= \left(\mathbf{TM}_{01} + i\mathbf{TE}_{01}\right)/\sqrt{2} \end{aligned} \tag{1}$$

where $\mathbf{F}_{11}^{+}$ and $\mathbf{F}_{11}^{-}$ are fundamental modes with right and left-hand circular polarization, respectively. $\mathbf{F}_{21}^{+-}$ and $\mathbf{F}_{T21}^{+-}$ are high-order modes.

Evolution of the input pulses in the fiber is described by using the multimode generalized nonlinear Schrödinger equation (MM-NLSE) [39,40], as given in Eq. (2):

$$\begin{aligned} \frac{\partial A_p}{\partial z} = D\left\{A_p\right\} + \frac{i n_2 \omega_0}{c}\left(1 + \frac{i}{\omega_0}\frac{\partial}{\partial t}\right)\sum_{l,m,n}\Big\{\left(1 - f_R\right) S_{plnm}^{K} A_l A_m A_n^* \\ + f_R S_{plnm}^{R} A_l\left[h * \left(A_m A_n^*\right)\right]\Big\}, \end{aligned} \tag{2}$$

where A_p is amplitude in mode p; f_R is Raman fraction; S_{plnm}^{K} and S_{plnm}^{R} are the overlap integrals, indicating the interaction between the mode via instantaneous (Kerr) and noninstantaneous nonlinearity, respectively. Nonlinear refractive index n_2 and Raman fraction f_R of CS_2 depend on pulse duration of laser pumps [24]. For example, values of $\{n_2, f_R\}$ at pulse duration of 100 fs, 200 fs and 300 fs are: $\{3 \times 10^{-19}, 0.5\}$, $\{5 \times 10^{-19}, 0.7\}$, and $\{7.5 \times 10^{-19}, 0.8\}$, respectively [24], in which n_2 is given in unit of $m^2\ W^{-1}$.

Eq. (2) is formulated under the assumptions that: (i) the response/variation of the pulse amplitude and the nonlinear coefficients is much lower than a single cycle of the carrier wave and (ii) the shock time $\tau_0 = 1/\omega_0$ remains constant for all combination modes and polarization states [40].

Table 2
Nonlinear parameters of carbon disulfide [24,42,43].

Parameters	Values	Parameters	Values
$n_{2d\parallel}$ $(10^{-19}\ m^2\ W^{-1})$	18	$t_{r,c}$ (ps)	0.15
$n_{2I\parallel}$ $(10^{-19}\ m^2\ W^{-1})$	7.6	$t_{f,c}$ (ps)	0.14
$n_{2c\parallel}$ $(10^{-19}\ m^2\ W^{-1})$	1.0	$t_{f,I}$ (ps)	0.45
$n_{2d\perp}$ $(10^{-19}\ m^2\ W^{-1})$	−9.44	ω_0 (ps^{-1})	8.5
$n_{2I\perp}$ $(10^{-19}\ m^2\ W^{-1})$	−3.73	σ (ps^{-1})	5
$N_{2\parallel}$ $(10^{-19}\ m^2\ W^{-1})$	26.6	$t_{\perp 0}$ (ps)	0.1
$N_{2\perp}$ $(10^{-19}\ m^2\ W^{-1})$	13.17	$t_{\perp}^{d}$ (ps)	0.107
$t_{r,d}$ (ps)	0.15	$t_{\perp}^{I}$ (ps)	1.281
$t_{f,d}$ (ps)	1.61		

The first term of right-hand in Eq. (2) describes the linear effects, e.g., loss, dispersion, relative delay between the modes, as given in Eq. (3):

$$D\left\{A_p\right\} = i\left(\beta_0^{(p)} - \beta_0\right)A_p - \left(\beta_1^{(p)} - \beta_1\right)\frac{\partial A_p}{\partial t} - \frac{\alpha^p}{2}A_p + i\sum_{n\geq 2}\frac{\beta_n^{(p)}}{n!}\left(i\frac{\partial}{\partial t}\right)^n A_p. \tag{3}$$

The first term of the right-hand of Eq. (3) describes phase variation, the second term is relative delay between the modes, α^p is fiber loss at mode p, and the last term is dispersion effect. The free parameters β_0 and β_1 are chosen to present the propagation constant and group velocity, respectively, of the fundamental mode ($HE_{11,x}$).

S_{plnm}^{K} and S_{plnm}^{R} factors are given by Eqs. (4) and (5) [40]:

$$S_{plmn}^{R} = \frac{\int dx\,dy\,[\mathbf{F}_p^*.\mathbf{F}_l][\mathbf{F}_m.\mathbf{F}_n^*]}{\left[\int dx\,dy\,|\mathrm{F}_p|^2 \int dx\,dy\,|\mathrm{F}_l|^2 \int dx\,dy\,|\mathrm{F}_m|^2 \int dx\,dy\,|\mathrm{F}_n|^2\right]^{1/2}}, \tag{4}$$

$$\begin{aligned} S_{plmn}^{K} &= \frac{2}{3}S_{plmn}^{R} \\ &+ \frac{1}{3}\frac{\int dx\,dy\,[\mathbf{F}_p^*.\mathbf{F}_n^*][\mathbf{F}_m.\mathbf{F}_l]}{\left[\int dx\,dy\,|\mathrm{F}_p|^2 \int dx\,dy\,|\mathrm{F}_l|^2 \int dx\,dy\,|\mathrm{F}_m|^2 \int dx\,dy\,|\mathrm{F}_n|^2\right]^{1/2}}, \end{aligned} \tag{5}$$

where $\mathbf{F}_{p,l,m,n}$ is electric field functions of modes p, l, m, n, respectively.

In Eq. (2), the Raman response function h of CS_2 depends on the difference in polarization between A_m and A_n modes. In particular, if A_m and A_n have linear polarization, and their polarization are orthogonal to each other, the formation of h is given by Eq. (6) [33]:

$$h = h_{\perp} = \frac{1}{N_{2\perp}}\sum_{i=d,I}\left[n_{2i\perp}\frac{1}{t_{\perp}^{i} - t_{\perp 0}}\left(\exp\left(\frac{-t}{t_{\perp}^{i}}\right) - \exp\left(\frac{-t}{t_{\perp 0}}\right)\right)\right]. \tag{6}$$

For other cases of the relative relationship of polarization states between the A_m and A_n modes (i.e., parallel and circular polarization), h is given as in Eq. (7) [24,33]:

$$\begin{aligned} h = h_{\parallel} = \frac{1}{N_{2\parallel}}\Bigg[n_{2I\parallel}\exp\left(\frac{-t}{t_{f,I}}\right)\int_0^{\infty}\frac{\sin(\omega t)}{\omega}\mathrm{g}(\omega)\,d\omega \\ + \sum_{k=c,d} n_{2k\parallel}\left(1 - \exp\left(\frac{-t}{t_{r,k}}\right)\right)\exp\left(\frac{-t}{t_{f,k}}\right)\Bigg], \end{aligned} \tag{7}$$

where $\mathrm{g}(\omega)$ is the distribution function of librational motion as shown in Eq. (8) [41]:

$$\mathrm{g}(\omega) = \exp\left[\frac{\left(\omega - \omega_0\right)^2}{2\sigma^2} - \frac{\left(\omega - \omega_0\right)^2}{2\sigma^2}\right]. \tag{8}$$

All nonlinear parameters of CS_2 are summarized and shown in Table 2.

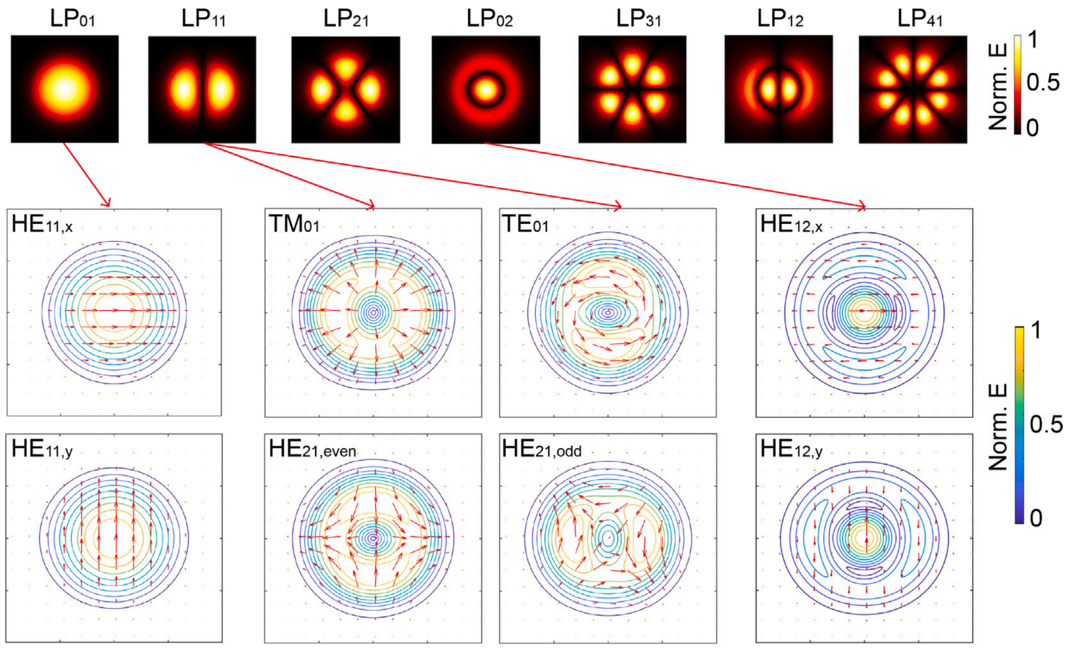

Fig. 2. The scalar modes (LP_{mn} modes) in the CS_2-core fiber at 1560 nm and examples of vector modes corresponding to LP_{01}, LP_{11}, LP_{02}. The arrows indicate the electrical field vector.

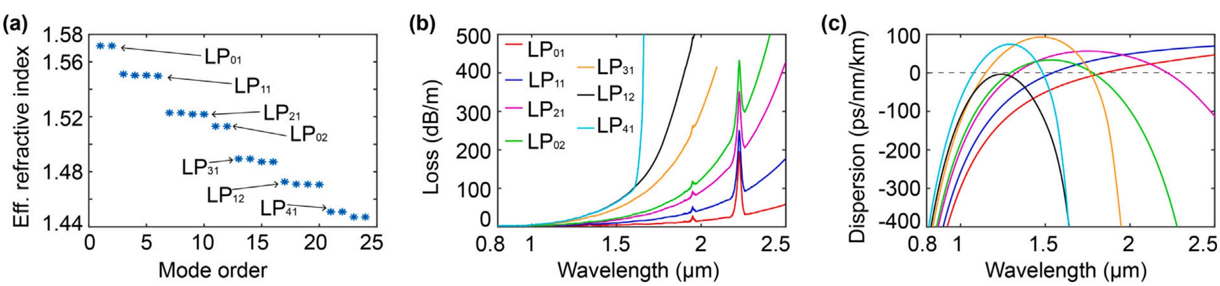

Fig. 3. (a) Effective refractive index of the fiber modes, (b) loss and (c) dispersion of LP_{mn} modes in the fiber.

In this work, we also consider the coherence of output spectra of selected modes via effects of vacuum noise [1], as given in Eq. (9):

$$\left|g_{12}^{1}\right| = \left|\frac{A_{p,1}^{*}(\omega)A_{p,2}(\omega)}{\left[\left|A_{p,1}(\omega)\right|^{2}\left|A_{p,2}(\omega)\right|^{2}\right]^{1/2}}\right|, \tag{9}$$

where p is a selected mode. The coherence is calculated with 20 simulations with random phase noises, resulting in 190 pairs $\{A_{p,1}, A_{p,2}\}$.

3. Supercontinuum generation in the fiber

SC generation in the liquid-core fiber is numerically simulated by using a split-step Fourier method to solve Eq. (2), in which we choose a time window: 21.5 ps; a number of time-frequency points: 2^{13}; and a step of fiber length: 72 μm. The laser has a central wavelength of 1560 nm and a pulse duration of 100 fs. The fiber length is 10 cm.

3.1. Supercontinuum generation in the fundamental mode

3.1.1. Interaction between the linearly polarized modes $HE_{11,x}$ and $HE_{11,y}$

Almost previous works studied SC generation in liquid-core fibers with the assumption of single-mode operation, i.e., using the scalar nonlinear Schrödinger equation [17,18,21,35]. In such a case, only the fundamental scalar mode LP_{01} is assumed to be excited. However, the low birefringence of liquid-core fibers causes a strong interaction between the polarized components of the fundamental mode. Consequently, the vacuum noise is significantly amplified via polarization modulation instability (PMI) [44]. In this work, before investigating the interaction of all existing modes, we investigate the interaction between the linearly polarized fundamental modes $HE_{11,x}$ and $HE_{11,y}$ with linear polarization input laser pulses.

Input laser pulses with linear polarization are characterized by their electric field vector located in a single plane. These linearly polarized pulses are typically emitted by commercial femtosecond lasers and can be tuned using a half-wave plate. Because the output pulses from these lasers are spatially distributed in a bell-shaped intensity profile, the majority of the input light energy is coupled into the fundamental modes with linear polarization (i.e., $HE_{11,x}$ or $HE_{11,y}$). However, during propagation along the fiber, the polarization state may change due to mode interactions.

Interestingly, as mentioned in Section 2, CS_2 has a high value of Raman fraction ($f_R = 0.5$ for a pulse duration of 100 fs). This indicates that, compared to solid-core fibers, a larger portion of the input pulse energy is utilized for the Raman effect. To emphasize the unique properties of mode interaction in the liquid core fiber, we compare its nonlinear propagation with that of a solid-core fiber made from non-silica glasses, such as PBG glass with $n_2 = 2\times10^{-19}$ m^2 W^{-1} and

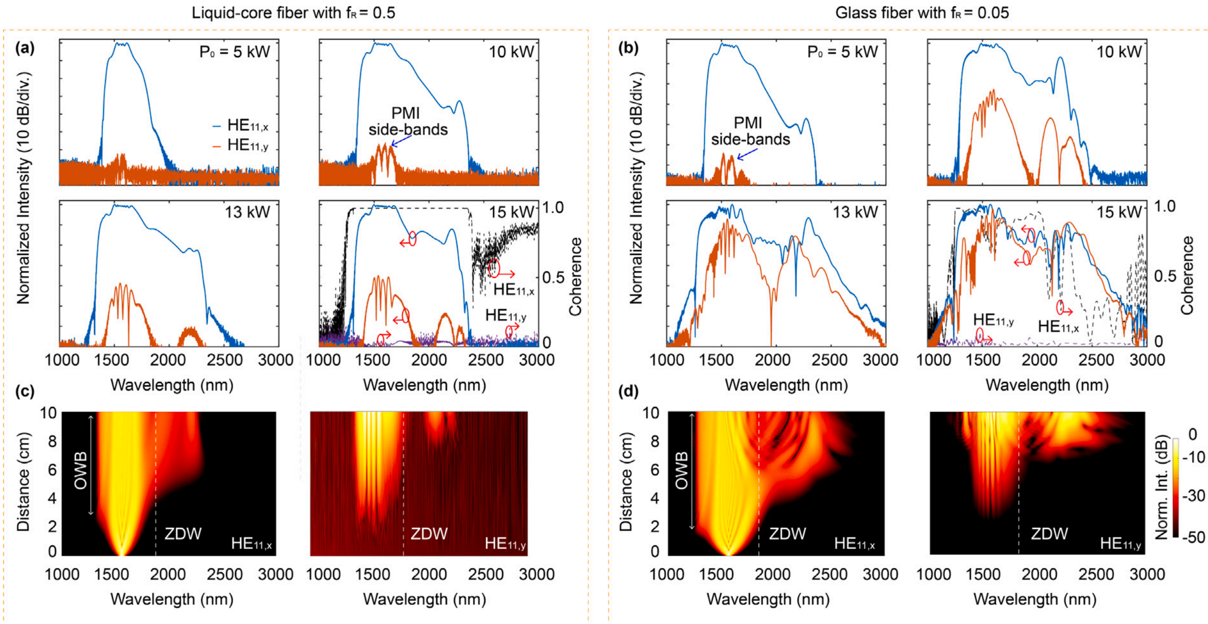

Fig. 4. (a) SC spectrum in the liquid-core fiber with various input peak powers—the considered modes are linear-polarized fundamental modes $HE_{11,x}$ and $HE_{11,y}$, (b) SC in the solid-core fiber with the same modes, (c) evolution of laser pulses in the liquid-core fiber with an input peak power of 15 kW, (d) the same for the solid-core fiber.

$f_R = 0.05$ [45]. Note that the solid-core fiber is assumed to have similar linear properties (e.g., mode dispersion and spatial mode distributions) to the liquid-core fiber.

The liquid core fiber is low birefringent and it does not have particular polarization axes (i.e., fast and slow axis). Therefore, we assume that the x- and y-axis (accordingly to $HE_{11,x}$ and $HE_{11,y}$ mode) is parallel and orthogonal to the electric vector of the input pulses, respectively. In such a case, almost all input powers are launched into $HE_{11,x}$.

For linear polarization, the interaction between the vector modes (also referred to as linear-polarized modes) is increased over the input powers as illustrated in Fig. 4(a,b). At low input power (P_0 = 5 kW), most of the light energy remains in the excited mode ($HE_{11,x}$) and very small portion energy is transferred into another mode due to PMI. In this case, PMI spectral sidebands are observed around the pump. For the liquid-core fiber, the interaction between fundamental modes remains low even at high input power (15 kW), with the spectral intensity of $HE_{11,y}$ being 30 dB lower than that of $HE_{11,x}$. Consequently, SC generation in the excited mode $HE_{11,x}$ exhibits high coherence, with $|g_{12}^1| = 1$ over the entire spectrum (see Fig. 4(a) with input peak power of 15 kW).

In contrast, the solid-core fiber with $f_R = 0.05$ has a strong interaction between the vector modes at high input peak power (e.g., 13 kW and 15 kW), resulting in a significant energy transfer from the excited mode ($HE_{11,x}$) to $HE_{11,y}$. Consequently, spectral intensities across the entire spectrum of the $HE_{11,y}$ mode are close to those of the $HE_{11,x}$ mode. In this scenario, the coherence of SC in the excited mode ($HE_{11,x}$) slightly decreases, shown in Fig. 4(b) with input peak power of 15 kW.

Interestingly, the coherence of the $HE_{11,y}$ mode is extremely low (i.e., $|g_{12}^1| \approx 0$ over the entire spectrum) for both cases of liquid-core and solid-core fibers, as illustrated in Fig. 4(a, b) with input peak power of 15 kW. This can be attributed to the spectrum of the $HE_{11,y}$ mode starting with PMI and further evolving due to noise-driven effects.

The nonlinear dynamics of pulse evolution in the investigated fibers are depicted in Fig. 4(c,d) with an input power of 15 kW. Since the pump wavelength is located in the normal dispersion regime, self-phase modulation (SPM) and optical wave breaking (OWB) primarily contribute to the pulse broadening of the excited mode ($HE_{11,x}$) at the onset of nonlinear propagation. As the spectrum exceeds the ZDW at 1850 nm, Raman frequency shifting and FWM create new wavelengths at the leading edge [46]. The interaction between the modes transfers energy from the excited mode to another mode, with PMI side bands appearing around 2 cm and 3 cm in the liquid-core and solid-core fibers, respectively.

3.1.2. Interaction between the circularly polarized modes F_{11}^+ and F_{11}^-

Unlike linear polarization, circularly polarized laser pulses have an electric field vector that rotates at a constant rate within a plane, while maintaining a constant magnitude. Experimentally, circular polarization can be achieved by using a quarter-wave plate.

For circular polarization, we investigate the nonlinear propagation and interaction between the circularly polarized fundamental modes F_{11}^+ and F_{11}^-, assuming that all input energy is coupled into the F_{11}^+ mode.

The overlap integrals of Kerr nonlinearity (S_{plmn}^K) are calculated using the spatial mode distributions outlined in Eq. (1). Employing Eqs. (4) and (5), our calculations yield the values of the elements of S_{plmn}^K, which are approximately 2/3 of S_{plmn}^R. For example, $S_{1111}^K = 5.36\times 10^{10}$, while $S_{1111}^R = 8.04\times10^{10}$. This ratio of 2/3 is a well-agreement with predictions from previous research in Ref. [40]. Thus, we investigate the nonlinear propagation in fibers with an input peak power of 23 kW to approximate the Kerr effects observed in linear-polarized modes with an input peak power of 15 kW.

The nonlinear dynamics for spectral broadening are similar to those of the linear-polarized modes, as shown in Fig. 5(c, d). However, interestingly, the circularly polarized fundamental modes do not significantly interact with each other, resulting in the intensity of the F_{11}^- mode remaining at the noise level. This reduces coherence degradation caused by PMI effects. Consequently, the SC generation of the F_{11}^+ mode exhibits high coherence, with $|g_{12}^1| = 1$ across the entire spectrum, as illustrated in Fig. 5.

With a given input peak power, the spectral bandwidth provided by the liquid-core fiber is narrower compared to that of the solid-core fiber. For instance, considering a 20 dB dynamic range, the spectral bandwidths provided by the liquid-core and solid-core fibers with an input peak power of 15 kW are 920 nm (from 1340 to 2260 nm) and 1160 nm (from 1260 to 2420 nm), respectively (see Fig. 4(a,b)). This characteristic also holds for circularly polarized modes, as depicted in Fig. 5(a,b).

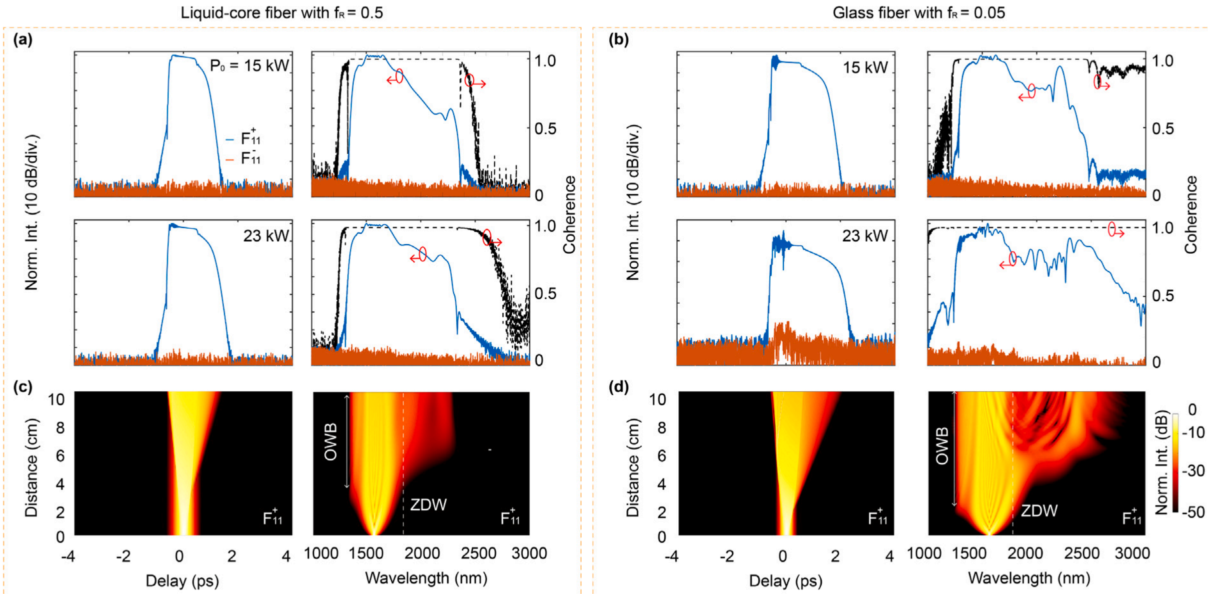

Fig. 5. (a) SC spectrum in the liquid-core fiber with various input peak powers—the considered modes are circular-polarized fundamental modes (F^{+}_{11} and F^{-}_{11}), (b) SC in the solid-core fiber with the same modes, (c) temporal and spectral evolution of a laser pulse in F^{+}_{11} mode in the liquid-core fiber with an input peak power of 23 kW, (d) the same for the solid-core fiber.

The narrow spectral bandwidth observed in the liquid-core fiber is attributed to its high Raman fraction ($f_R = 0.5$), which results in a small portion of the initial input power being utilized for Kerr nonlinearity, as illustrated in Eq. (2). Consequently, the spectrum induced by self-phase modulation, which depends on Kerr nonlinearity, has a narrower bandwidth. Regarding further nonlinear dynamics, at the trailing edge, optical wave breaking occurs only when SPM-induced components temporally overlap with the pulse tail [47]. At the leading edge, the narrow SPM-induced spectrum in the liquid-core fiber results in only a small portion of the spectrum exceeding the ZDW for soliton dynamics. This feature also concludes that the spectral bandwidth of normal-dispersion SC generation significantly depends on the initial spectral bandwidth induced by SPM.

3.2. Supercontinuum generation in the first high-order modes LP_{11}

The first high-order modes LP_{11} in a liquid-core fiber can be experimentally excited using an s-waveplate and a half-wave plate. The s-waveplate transforms a linearly polarized Gaussian beam into a ring-shaped beam. Depending on the polarization state of the input beam, a desired mode (i.e., $HE_{11,even/odd}$, TM_{01}, and TE_{01}) is excited [31].

We investigate nonlinear propagation in liquid-core fibers, assuming that only $HE_{21,odd}$ or TM_{01} is initially excited. We do not consider the interaction of these modes with other higher-order modes due to the heavy workload of the simulation process. Moreover, the interaction between the first high-order modes and other modes is weak due to low overlap integral [48].

Our results indicate that there is no nonlinear interaction between the first higher-order modes and the fundamental modes for both linear and circular polarization. This implies that the intensities of the fundamental modes are at noise levels.

The nonlinear propagation in liquid-core fibers depends on the initially excited modes. Specifically, when an input beam is coupled into the $HE_{21,odd}$ mode, the light energy is transferred only to the TM_{01} mode, as illustrated in Fig. 6. The light intensities of other high-order modes ($HE_{21,odd}$ and TE_{01}) are at noise levels (not shown here). The spectral intensities of the TM_{01} mode are much lower (30 dB) than that of the $HE_{21,odd}$ mode, as depicted in Fig. 6(a,b). The temporal profiles shift to positive delays over the propagation distance, because the high-order modes have smaller group velocity dispersion compared to the fundamental modes, as seen in Fig. 6(c,d). At 10 cm of the propagation, the temporal profiles are completely located in the positive delay, as shown in Fig. 6(a,b).

When an input beam is coupled into the TM_{01} mode, the light energy is transferred to two modes ($HE_{21,odd}$ and TE_{01}), as shown in Fig. 7(b,c). The intensities of TE_{01} mode are created after 4 cm of propagation. It is also notable that there is no interaction between these modes and $HE_{21,even}$.

The intensities of the $HE_{21,odd}$ and TE_{01} modes are much lower than that of the excited mode, implying that the spectro-temporal properties of the output spectra strongly depend on the nonlinear dynamics occurring in single mode guidance (TM_{01} mode) with anomalous dispersion, as discussed in previous work [1]. Within this framework, the first high-order modes have a ZDW at 1545 nm; thus, the pump wavelength at 1560 nm is located in the anomalous dispersion region, resulting in soliton formation through a balance between SPM and dispersion. Since the pump wavelength is close to the ZDW, the pulse significantly experiences the effects of high-order dispersion, such as soliton radiation induced by third-order dispersion [49]. Soliton fission occurs around 3 cm of propagation, providing a broad spectral bandwidth (1100–2300 nm), Figs. 6(a) and 7(a).

Unlike linearly polarized modes, circular polarization induces mode interaction between the excited mode and all vector modes of LP_{11}. For example, when the F^{-}_{21} mode is initially excited, mode interaction generates intensities in the other three modes: F^{+}_{21}, F^{+}_{T21}, and F^{-}_{T21}, as illustrated in Fig. 8(a–d). This characteristic contrasts with the behavior of circularly polarized fundamental modes, as shown in Fig. 5, where no interaction occurs between an excited fundamental mode and another one.

Similarly, as mentioned earlier, there is no interaction between the first high-order modes and the fundamental modes (F^{+}_{11} and F^{-}_{11}). Consequently, the intensities at the fundamental modes remain at the noise level, as depicted in Fig. 8(e).

Although the scenario of mode interaction differs for each selected mode excitation and polarization situation, the output spectra appear similar in terms of bandwidth and spectral structure for all investigated cases involving the first high-order modes, as depicted in Figs. 6(a), 7(a), and 8(d). The reason for this similarity lies in the significantly lower values of the intermodal intensities compared to those of the

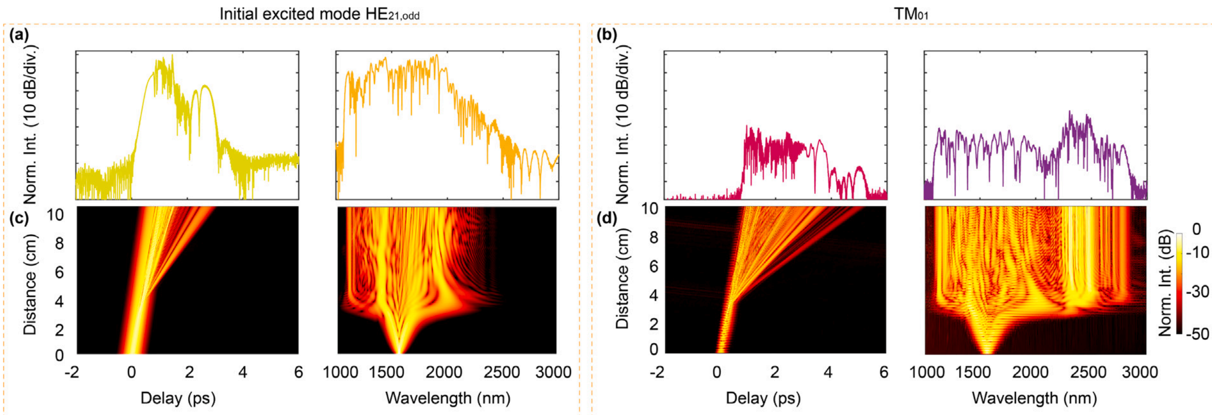

Fig. 6. SC spectrum in the liquid-core fiber with the linearly polarized higher-order modes. The initially excited mode is $HE_{21,odd}$. (a) Spectro-temporal evolution, spectral output, and temporal output of the excited mode $HE_{21,odd}$, (b) the same for TM_{01}.

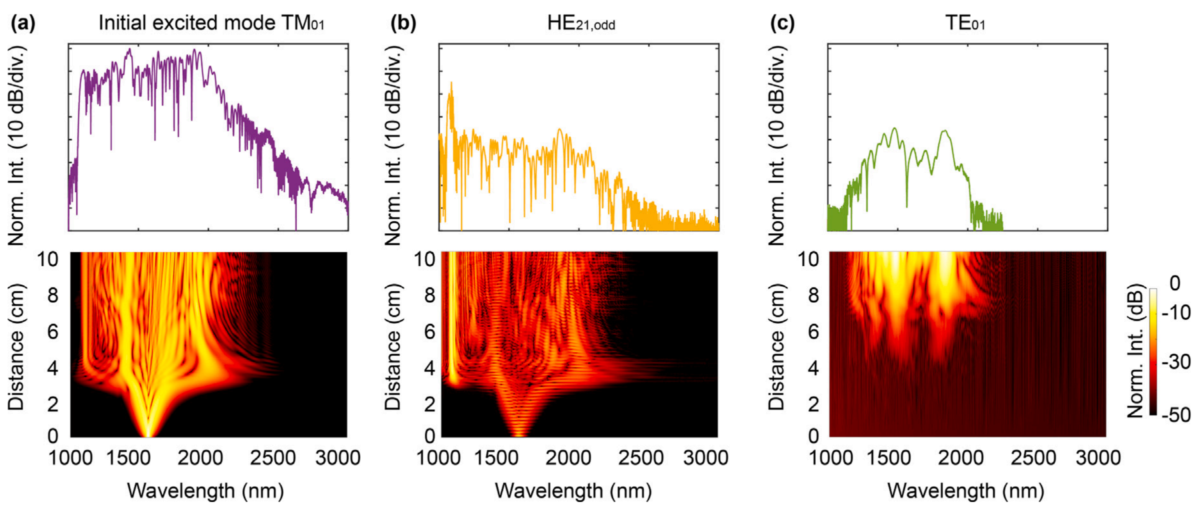

Fig. 7. SC spectrum in the liquid-core fiber with the linearly polarized higher-order modes. The initially excited mode is TM_{01}. (a) Spectral evolution and spectral output of the excited mode TM_{01}, (b) and (c) the same for $HE_{21,odd}$ and TE_{01}, respectively.

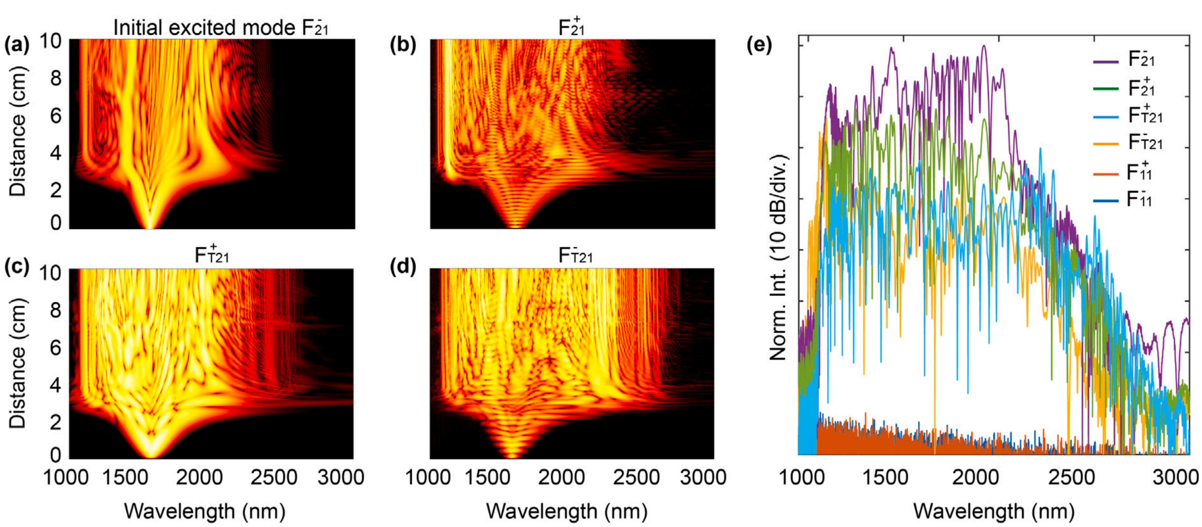

Fig. 8. SC spectrum in the liquid-core fiber with the circularly polarized higher-order modes. The initially excited mode is F^{-}_{21}. (a–d) Spectral evolution of the modes F^{-}_{21}, F^{+}_{21}, F^{+}_{T21}, F^{-}_{T21}, respectively; (e) output spectra of these modes.

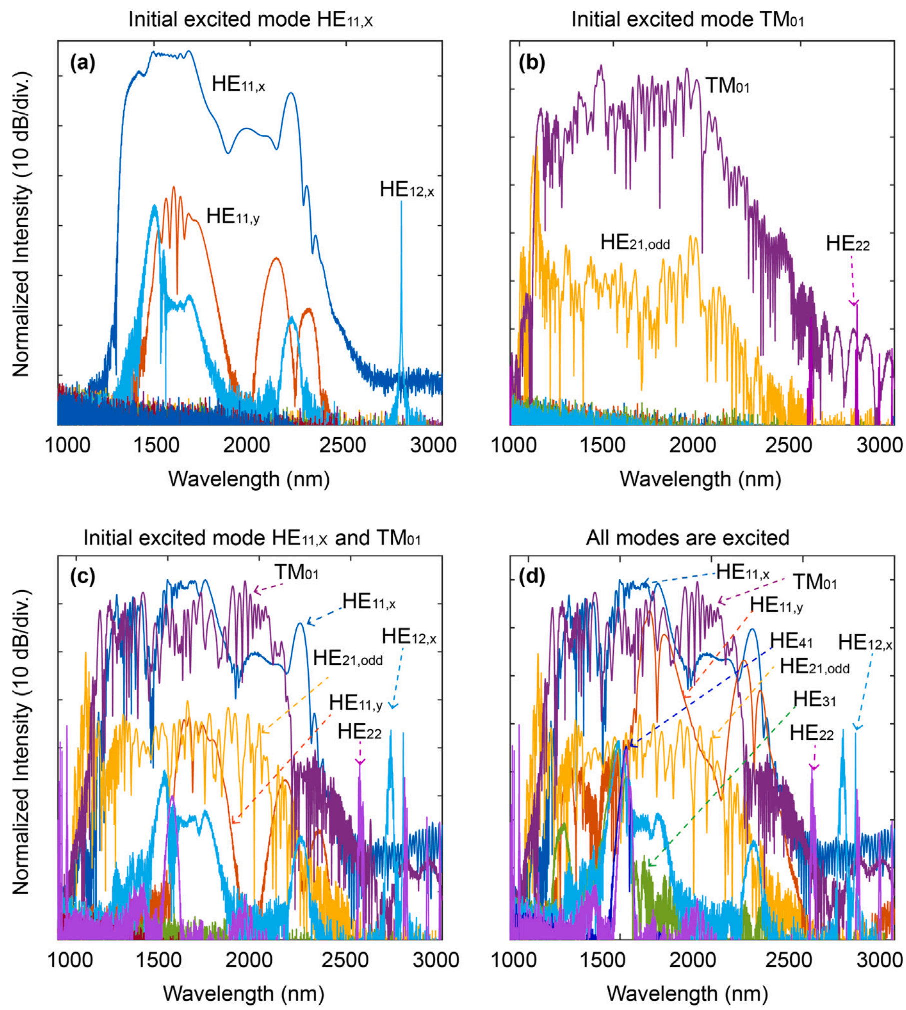

Fig. 9. SC spectrum in the liquid-core fiber with the linearly polarized modes. The 8 considered modes are $HE_{11,x}$, $HE_{11,y}$, TM_{01}, $HE_{21,odd}$, HE_{31}, $HE_{12,x}$, HE_{41}, HE_{22}. (a) SC with initial excited mode of $HE_{11,x}$; (b) with TM_{01}; (c) with both $HE_{11,x}$ and TM_{01}; (d) all modes are excited.

excited mode. Therefore, the output spectra strongly depend on the nonlinear phenomena, specifically soliton dynamics, occurring in the excited mode. The soliton-induced SC generation of the first high-order modes exhibits low coherence, with an average value of $\langle g_{12}^{1} \rangle = 0.25$, due to vacuum noise amplified by MI and PMI.

3.3. Interaction between all the modes

The aforementioned sections consider the interaction between the polarization components of fundamental and the first high-order LP_{nm} modes. Indeed, the fibers offer only fundamental mode (LP_{01}) and/or the first high-order (LP_{11}) require small core diameters and low contrast of refractive index between the core and cladding. For fibers with large cores, they offer multimode guidance, and thus, further high-order modes causes significant changing spectro-temporal properties of SC generation. Previous work studied the interaction between fundamental and high-order modes for silica fibers [48].

For the investigated liquid core fiber, there are 24 modes belonging to 7 modes LP_{nm}, as shown in Fig. 2. In this work, we assume that excited modes are $HE_{11,x}$ and TM_{01}, meaning that initial input laser pulses are coupled into either $HE_{11,x}$ and/or TM_{01}.

The interaction between each $HE_{11,x}$ and TM_{01} with each high-order mode are preliminary studied as shown in Appendix. The results show that (i) there is no interaction between the selected modes and any polarization component of the LP_{41} mode, thus the LP_{41} mode will not be considered for nonlinear interaction in the subsequent section; (ii) the selected modes ($HE_{11,x}$, TM_{01}) interact with only one polarization component of the high-order LP_{mn} modes, and these corresponding components are therefore chosen to characterize nonlinear propagation in the fiber.

For the numerical simulation of nonlinear propagation, we did not consider possible interactions of all 24 modes because of time consumption. To reduce the computational time, we considered interaction between the 8 modes, which are $HE_{11,x}$, $HE_{11,y}$, TM_{01}, $HE_{21,odd}$, $HE_{31,odd}$, $HE_{12,x}$, $HE_{41,odd}$, HE_{22}. The 8 modes are selected by using results in the aforementioned sections and preliminary study as shown in Appendix, while the contribution of other modes to nonlinear propagation is negligible if initial excited modes are either $HE_{11,x}$ or TM_{01}.

The interaction between the modes is mediated by intermodal FWM and cross-phase modulation (XPM), which can be estimated through the values of S^{K}_{plnm} and S^{R}_{plnm} coefficients as given in Eqs. (4) and (5). With an input peak power of 15 kW, if only $HE_{11,x}$ is excited, the power is transferred solely to $HE_{11,y}$ and $HE_{12,x}$ modes. The $HE_{12,x}$ is phase-locked with the pump due to the same symmetry class (i.e., distribution profile of electric field) and large spatial overlap with the $HE_{11,x}$ mode, see Fig. 9(a). If only the TM_{01} mode is excited, the power is transferred to $HE_{21,odd}$ and HE_{22} modes, as depicted in Fig. 9(b). However, the HE_{22} mode has high loss at long wavelengths, resulting in a significant reduction of light intensities.

When both $HE_{11,x}$ and TM_{01} are initially pumped simultaneously, it gives rise to a more complex nonlinear process. These two modes can

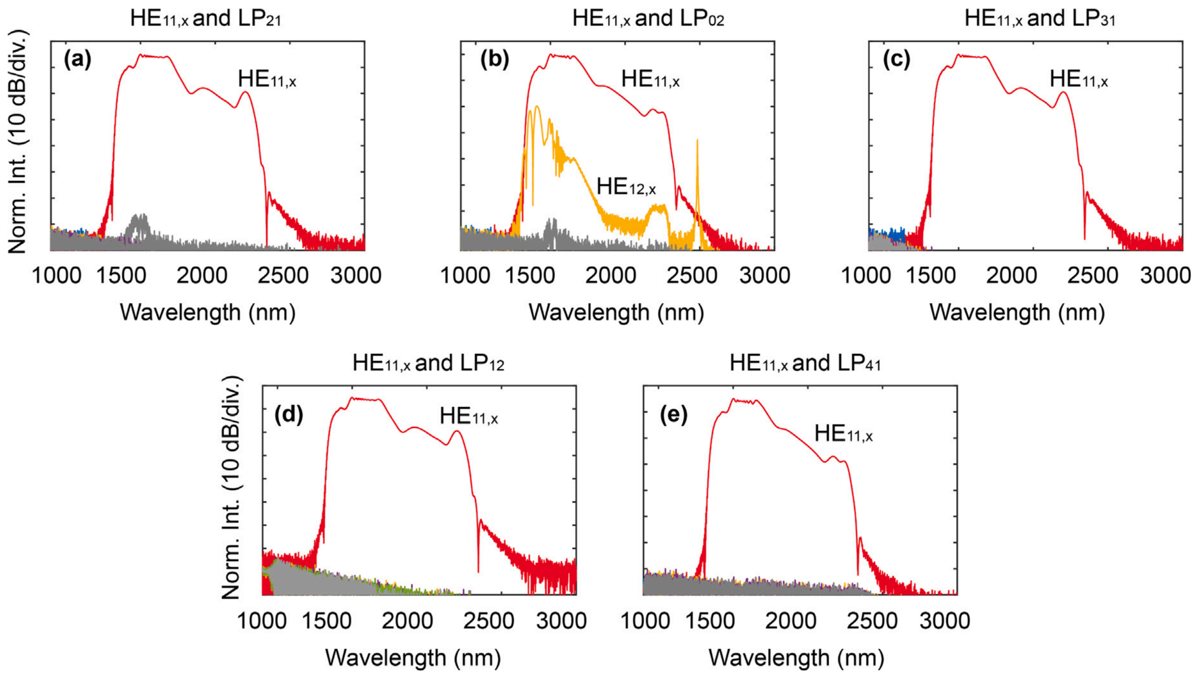

Fig. A.1. Spectra of $HE_{11,x}$ with all polarized components of each LP_{mn} mode. (a) interaction $HE_{11,x}$ and LP_{21}; (b) LP_{02}; (c) LP_{31}; (d) LP_{12}; and (e) LP_{41}. The initial excited mode for all the cases is $HE_{11,x}$ with input peak power of 15 kW and pulse duration of 100 fs.

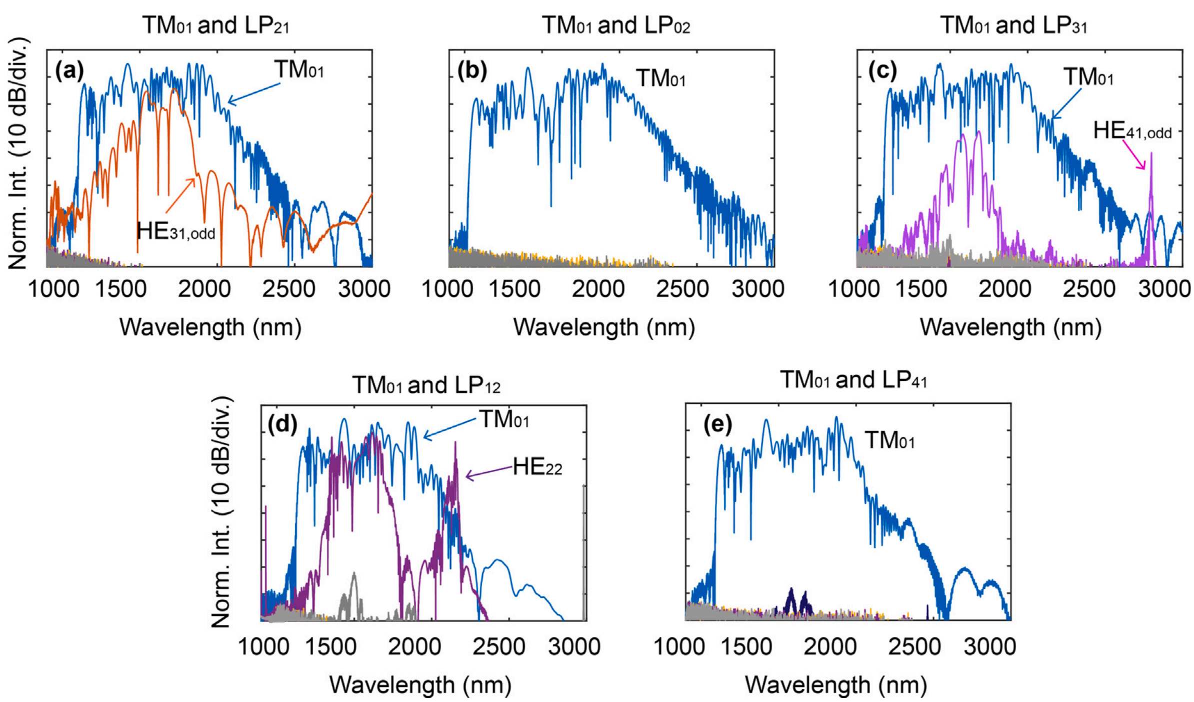

Fig. A.2. Spectra of TM_{01} with all polarized components of each LP_{mn} mode. (a) interaction TM_{01} and LP_{21}; (b) LP_{02}; (c) LP_{31}; (d) LP_{12}; and (e) LP_{41}. The initial excited mode for all the cases is TM_{01} with input peak power of 15 kW and pulse duration of 100 fs.

act as pumps for all other non-excited modes through FWM, resulting in a rapid increase in the intensities of the non-excited modes. In such a case, the spectral contrast between $HE_{21,odd}$ and TM_{01} is around 20 dB, lower than the case when only TM_{01} is excited (see Fig. 9(c)). The interaction between modes also leads to noise appearing in the spectrum of the $HE_{11,x}$ mode, potentially reducing coherence.

It is worth noting that all non-excited modes are initially empty, meaning they are not pumped at the beginning. This implies that their intensities are induced from noises by spontaneous FWM over the nonlinear propagation, resulting in slow spectrum development. However, if these modes are initially seeded with very low power, meaning they are pumped with very low power, the spectrum is created by simulated FWM rather than spontaneous FWM, leading to faster spectrum development. For instance, Fig. 9(d) presents the spectra of all modes when $HE_{11,x}$ and TM_{01} are initially pumped with a high peak power (15 kW) and 0.15 kW for others. Compared to the case in Fig. 9(c), $HE_{11,y}$ has a high intensity, and it is possible to observe peaks in the spectra for the HE_{31} and HE_{41} modes.

4. Conclusion

In this work, we investigate SC generation in a few-mode CS_2-core fiber with a 5 μm core diameter with femtosecond laser pulses. The fiber provides SC spectra with spectral bandwidth similar to previous works, as shown in Table 1. The novelty of our work is to investigate pulse broadening while considering the interaction of all existing modes (i.e., 24 modes) and the contribution of high noninstantaneous nonlinearity.

Although the fiber supports up to 24 polarized modes, the interactions between modes generally occur only between those with significant spatial overlap and similar polarization states. For example, if the $HE_{11,x}$ mode is initially excited, the light energy is transferred primarily to the $HE_{11,y}$ and $HE_{12,x}$ modes. This characteristic enables the optimization of SC generation properties by carefully selecting the initially excited mode.

Indeed, the input light from laser sources is typically coupled into the fundamental modes. In such a case, if only two polarized components of the fundamental mode are considered, the high noninstantaneous nonlinearity of the liquid results in a narrow spectral bandwidth but a high coherence of SC generation. Our study also pointed out that the interaction between the polarized components could be negligible if circular polarization is considered, improving the coherence of SC generation.

Understanding the nonlinear interaction between modes in liquid-core fibers is important for controlling the spectro-temporal properties of SC generation. Multimode fibers with a large core can be used for delivering high-power laser pulses. Along with a rich landscape of nonlinear phenomena caused by mode interaction, multimode liquid-core fibers have a high potential for applications requiring customizable SC generation and high power, such as multiphoton imaging techniques and absorption-based sensors.

CRediT authorship contribution statement

Lanh Chu Van: Writing – original draft, Methodology, Funding acquisition. **Hieu Le Van:** Investigation, Data curation. **Van Thuy Hoang:** Writing – review & editing, Writing – original draft, Supervision, Methodology, Conceptualization.

Declaration of competing interest

The authors declare that they have no known competing financial interests or personal relationships that could have appeared to influence the work reported in this paper.

Acknowledgments

This research is funded by Vietnam National Foundation for Science and Technology Development (NAFOSTED) under grant number 103.03–2023.01.

Appendix. Preliminary investigation of the interaction between $HE_{11,x}$ and TM_{01} with high-order modes

Since the simulation of the nonlinear propagation with all 24 modes in the fiber is time consumption, we first conduct preliminary calculations on the interaction between $HE_{11,x}$ and TM_{01} modes with all components of each LP_{mn} mode. The goal of this work is to determine which polarized components exhibit significant interaction with the $HE_{11,x}$ and TM_{01} modes. These polarized components will then be collected for analysis, as discussed in Section 3.3 of the main text.

The results indicate that the $HE_{11,x}$ mode does not exhibit significant interaction with the polarized components of the high-order LP_{mn} modes, except for $HE_{12,x}$, as shown in Fig. A.1(b). Consequently, the spectra of all the polarized modes are at noise levels, as seen in Fig. A.1(a, c, d, e).

For TM_{01} mode, it does not interact with LP_{02} because they do not have the same symmetry class, resulting in noise-level spectra of both polarized components of LP_{02}, see Fig. A.1(b). Whilst, TM_{01} mode experiences remarkably interaction with one component of other modes, LP_{mn} mode, e.g., $HE_{31,odd}$ of LP_{21}, $HE_{41,odd}$ of LP_{31}, and HE_{22} of LP_{12}, see Fig. A.2(a,c,d).

Both $HE_{11,x}$ and TM_{01} do not have noticeable power transferred to LP_{41} mode, as shown in Figs. A.1(e) and A.2(e).

Therefore, when either the $HE_{11,x}$ or TM_{01} modes are initially excited, the polarized components whose spectra are at noise level in both Figs. A.1 and A.2 are assumed to be ignored in the simulation, as discussed in Section 3.3 of the main text. The following modes are selected for consideration in this section: $HE_{11,x}$, $HE_{11,y}$, TM_{01}, $HE_{21,odd}$, $HE_{31,odd}$, $HE_{12,x}$, $HE_{41,odd}$, and HE_{22}.

Data availability

No data was used for the research described in the article.

References

[1] J.M. Dudley, G. Genty, S. Coen, Supercontinuum generation in photonic crystal fiber, Rev. Modern Phys. 78 (2006) 1135.
[2] C. Poudel, C. Kaminski, Supercontinuum radiation in fluorescence microscopy and biomedical imaging applications., J. Opt. Soc. Am. B 36 (2019) A139–A153.
[3] V.T. Hoang, Y. Boussafa, L. Sader, S. Février, V. Couderc, W. B., Optimizing supercontinuum spectro-temporal properties by leveraging machine learning towards multi-photon microscopy, Front. Photonics 3 (2022) 940902.
[4] A.M. Heidt, J.M. Hodasi, A. Rampur, D.M. Spangenberg, M. Ryser, M. Klimczak, T. Feurer, Low noise all-fiber amplification of a coherent supercontinuum at 2 μm and its limits imposed by polarization noise, Sci. Rep. 10 (2020) 16734.
[5] N. Picqué, T.W. Hänsch, Frequency comb spectroscopy, Nat. Photonics 13 (2019) 146–157.
[6] T. Udem, R. Holzwarth, T.W. Hänsch, Optical frequency metrolog, Nature 416 (2002) 233–237.
[7] T. Sylvestre, E. Genier, A.N. Ghosh, P. Bowen, G. Genty, J. Troles, A. Mussot, A.C. Peacock, M. Klimczak, A.M. Heidt, J.C. Travers, O. Bang, J.M. Dudley, Recent advances in supercontinuum generation in specialty optical fibers [invited], J. Opt. Soc. Am. B 38 (2021) F90–F103.
[8] C.R. Petersen, U. Møller, I. Kubat, B. Zhou, S. Dupont, J. Ramsay, T. Benson, S. Sujecki, N. Abdel-Moneim, Z. Tang, D. Furniss, A. Seddon, B. O., Mid-infrared supercontinuum covering the 1.4–13.3 μm molecular fingerprint region using ultra-high NA chalcogenide step-index fibre, Nat. Photonics 8 (2014) 830–834.
[9] L. Chen, M. Liao, W. Bi, F. Yu, T. Wang, W. Gao, L. Hu, Coherent supercontinuum generation in step-index heavily ge-doped silica fibers with all normal dispersion, IEEE Photonics J. 14 (2022) 7136106.
[10] T.L. Canh, V.T. Hoang, H.L. Van, D. Pysz, V.C. Long, T.B. Dinh, D.T. Nguyen, Q.H. Dinh, M. Klimczak, R. Kasztelanic, J. Pniewski, R. Buczynski, K.X. Dinh, Supercontinuum generation in all-normal dispersion suspended core fiber infiltrated with water, Opt. Mater. Express 10 (2020) 1733–1748.
[11] C. Lafforgue, M. Montesinos-Ballester, T.T.D. Dinh, X.L. Roux, E. Cassan, D. Marris-Morini, C. Alonso-Ramos, L. Vivien, Supercontinuum generation in silicon photonics platforms, Photonics Res. 10 (2022) A43–A56.
[12] A. Lemière, R. Bizot, F. Désévédavy, G. Gadret, J.C. Jules, P. Mathey, C. Aquilina, P. Béjot, F. Billard, O. Faucher, B. Kibler, F. Smektala, 1.7–18 μm mid-infrared supercontinuum generation in a dispersion-engineered step-index chalcogenide fiber, Results Phys. 26 (2021) 104397.
[13] P. Koštál, J. Shánělová, J. Málek, Viscosity of chalcogenide glass-formers, Int. Mater. Rev. 65 (2019) 63–101.
[14] P. Toupin, L. Brilland, D. Méchin, J.L. Adam, J. Troles, Optical aging of chalcogenide microstructured optical fibers, J. Lightwave Technol. 32 (2014) 2428–2432.
[15] A. Adamu, M.S. Habib, C.R. Petersen, J.E.A. Lopez, B. Zhou, A. Schülzgen, M. Bache, R. Amezcua-Correa, O. Bang, C. Markos, Deep-UV to mid-IR supercontinuum generation driven by mid-IR ultrashort pulses in a gas-filled hollow-core fiber, Sci. Rep. 9 (2019) 4446.
[16] M.F. Galán, J. Serrano, E.C. Jarque, R. Borrego-Varillas, M. Lucchini, M. Reduzzi, M. Nisoli, C. Brahms, J.C. Travers, C. Hernández-García, J.S. Roman, Robust isolated attosecond pulse generation with self-compressed sub-cycle drivers from hollow capillary fibers, 2023, arXiv:2312.13321.
[17] M. Chemnitz, M. Gebhardt, C. Gaida, F. Stutzki, J. Kobelke, J. Limpert, A. Tünnermann, M.A. Schmidt, Hybrid soliton dynamics in liquid-core fibres, Nat. Commun. 8 (2017).

[18] V.T. Hoang, R. Kasztelanic, A. Anuszkiewicz, G. Stepniewski, A. Filipkowski, S. Ertman, D. Pysz, T. Wolinski, K.D. Xuan, M. Klimczak, R. B., All-normal dispersion supercontinuum generation in photonic crystal fibers with large hollow cores infiltrated with toluene, Opt. Mater. Express 8 (2018) 3568–3582.

[19] R.M. Gerosa, A. Sudirman, L.d.S. Menezes, W. Margulis, C.J.S. de Matos, All-fiber high repetition rate microfluidic dye laser, Optica 2 (2015) 186–193.

[20] V.T. Hoang, D. Dobrakowski, G. Stępniewski, R. Kasztelanic, D. Pysz, K.X. Dinh, M. Klimczak, M. Śmietana, R. B., Antiresonant fibers with single- and double-ring capillaries for optofluidic applications, Opt. Express 28 (2020) 32483–32498.

[21] M. Chemnitz, R. Scheibinger, C. Gaida, M. Gebhardt, F. Stutzki, S. Pumpe, J. Kobelke, A. Tünnermann, A. Limpert, M.A. Schmidt, Thermodynamic control of soliton dynamics in liquid-core fibers, Optica 5 (2018) 695–703.

[22] S. Junaid, W. Huang, R. Scheibinger, K. Schaarschmidt, H. Schneidewind, P. Paradis, M. Bernier, R. Vallee, S. Stanca, G. Zieger, M. Schmidt, Attenuation coefficients of selected organic and inorganic solvents in the mid-infrared spectral domain, Opt. Mater. Express 12 (2022) 1754–1763.

[23] L.C. Van, N.V.T. Minh, B.T.L. Tran, T.D. Van, P.N.T. Hong, T.D. Mai, T.L. Canh, H.V. Le, T.N. Thi, T.T. Doan, V.T. Hoang, Broadband supercontinuum generation in cascaded tapered liquid core fiber, Opt. Commun. 537 (2023) 129441.

[24] P. Zhao, M. Reichert, S. Benis, D.J. Hagan, E.W.V. Stryland, Temporal and polarization dependence of the nonlinear optical response of solvents, Optica 5 (2018) 583–594.

[25] M. Chemnitz, Hybridization of solitons in realistic non-instantaneous fibers, Opt. Commun. 549 (2023) 129874.

[26] Z. Kang, F. Xu, J. Yuan, F. Li, B. Yan, X. Zhou, Q. Wu, K. Wang, X. Sang, K. Long, C. Yu, Slow-nonlinearity assisted supercontinuum generation in a CS2-core photonic crystal fiber, IEEE J. Quantum Electron. 55 (2019) 6800209, http://dx.doi.org/10.1109/JQE.2019.2901507.

[27] S. Kedenburg, M. Vieweg, T. Gissibl, H. Giessen, Linear refractive index and absorption measurements of nonlinear optical liquids in the visible and near-infrared spectral region, Opt. Mat. Express 2 (2012) 1588–1611.

[28] I. Cristiani, et al., Roadmap on multimode photonics, J. Opt. 24 (2022) 083001.

[29] T. Qiu, H. Cao, K. Liu, L. Yu, M. Levy, E. Lendaro, F. Wang, S. You, Spectral-temporal-spatial customization via modulating multimodal nonlinear pulse propagation, Nat. Commun. 15 (2024) 2031.

[30] C. Wang, G. Feng, W. Li, S. Zhou, Highly coherent supercontinuum generation in CS_2-infiltrated single-core optical fiber, J. Opt. 21 (2019) 105501, http://dx.doi.org/10.1088/2040-8986/ab3bb5.

[31] R. Scheibinger, N.M. Lüpken, M. Chemnitz, K. Schaarschmidt, J. Kobelke, C. Fallnich, M.A. Schmidt, Higher-order mode supercontinuum generation in dispersion-engineered liquid-core fibers, Sci. Rep. 11 (2021) 5270.

[32] C. Wang, K. Lin, S. Cao, G. Feng, J. Wang, A.N. Abdalla, Polarized supercontinuum generation in CS_2-core all-normal dispersion photonic crystal fiber, IEEE Photonics J. 14 (2022) 3061607, http://dx.doi.org/10.1109/JPHOT.2022.3223534.

[33] L.C. Van, B.T.L. Tran, T.D. Van, N.V.T. Minh, T.N. Thi, H.P.N. Thi, M.H.T. Nguyen, V.T. Hoang, Supercontinuum generation in highly birefringent fiber infiltrated with carbon disulfide, Opt. Fiber Technol. 75 (2023) 103151.

[34] C. Mei, G. Steinmeyer, J. Yuan, X. Zhou, K. L., Intermodal synchronization effects in multimode fibers with noninstantaneous nonlinearity, Phys. Rev. A 105 (2022) 013516.

[35] V.T. Hoang, R. Kasztelanic, A. Filipkowski, G. Stępniewski, D. Pysz, M. Klimczak, S. Ertman, V.C. Long, T.R. Woliński, M. Trippenbach, K.D. Xuan, M. Ś., R. Buczyński, Supercontinuum generation in an all-normal dispersion large core photonic crystal fiber infiltrated with carbon tetrachloride, Opt. Mater. Express 9 (2019) 2264–2278.

[36] V.T. Hoang, R. Kasztelanic, G. Stępniewski, K.D. Xuan, M. Trippenbach, M. Klimczak, R. Buczyński, J. Pniewski, Femtosecond supercontinuum generation around 1560 nm in hollow-core photonic crystal fibers filled with carbon tetrachloride, Appl. Opt. 59 (2020) 3720–3725, http://dx.doi.org/10.1364/AO.385003.

[37] H.C. Inc., Transmission calculator for optical applications, 2024, URL: https://www.heraeus-conamic.com/tools-and-services/tools/transmission-calculator/optical-applications.

[38] N. Bozinovic, S. Golowich, P. Kristensen, S. Ramachandran, Control of orbital angular momentum of light with optical fibers, Opt. Lett. 37 (2012) 2451–2453.

[39] F. Poletti, P. Horak, Description of ultrashort pulse propagation in multimode optical fibers, J. Opt. Soc. Am. B 25 (2008) 1645–1654.

[40] P. Horak, F. Poletti, Chapter 1: *Multimode Nonlinear Fibre Optics: Theory and Applications* in Recent Progress in Optical Fiber Research, InTech, 5 Princes Gate Court, London, SW7 2QJ, UK, 2012.

[41] M. Reichert, H. Hu, M.R. Ferdinandus, M. Seidel, P. Zhao, T.R. Ensley, D. Peceli, J.M. Reed, D.A. Fishman, S. Webster, D.J. Hagan, E.W.V. Stryland, Temporal, spectral, and polarization dependence of the nonlinear optical response of carbon disulfide, Optica 1 (2014) 436–445.

[42] Y. Sato, R. Morita, M. Yamashita, Study on ultrafast dynamic behaviors of different nonlinear refractive index components in CS_2 using a femtosecond interferometer, Japan. J. Appl. Phys. 36 (1997) 2109.

[43] Y. Sato, R. Morita, M. Yamashita, Femtosecond optical pulse compressor using CS_2 liquid-core fiber with negative delayed nonlinear response, Japan. J. Appl. Phys. 36 (1997) 6768.

[44] I.B. Gonzalo, R.D. Engelsholm, M.P. Sørensen, O. Bang, Polarization noise places severe constraints on coherence of all-normal dispersion femtosecond supercontinuum generation, Sci. Rep. 8 (2018) 6579, http://dx.doi.org/10.1038/s41598-018-24691-7.

[45] H.V. Le, V.T. Hoang, G. Stępniewski, T.L. Canh, N.V.T. Minh, R. Kasztelanic, M. Klimczak, J. Pniewski, K.X. Dinh, A.M. Heidt, R. Buczyński, Supercontinuum generation in an all-normal dispersion large core photonic crystal fiber infiltrated with carbon tetrachloride, Opt. Express 29 (2021) 39586–39600.

[46] V.P. Yanovsky, F.W. Wise, Nonlinear propagation of high-power, sub-100-fs pulses near the zero-dispersion wavelength of an optical fiber, Opt. Lett. 19 (1994) 1547–1549.

[47] A.M. Heidt, A. Hartung, G.W. Bosman, P. Krok, E.G. Rohwer, H. Schwoerer, H. Bartelt, Coherent octave spanning near-infrared and visible supercontinuum generation in all-normal dispersion photonic crystal fibers, Opt. Express. 19 (2011) 3775–3787.

[48] F. Poletti, P. Horak, Dynamics of femtosecond supercontinuum generation in multimode fibers, Opt. Express. 17 (2009) 6134–6147.

[49] P.K.A. Wai, H.H. Chen, Y.C. Lee, Radiations by "solitons" at the zero group-dispersion wavelength of single-mode optical fibers, Phys. Rev. A. 41 (1990) 426.